Plant and Soil **183:** 85–95, 1996.

pH mapping in transparent gel using color indicator videodensitometry

Benoît Jaillard, Laurent Ruiz and Jean-Claude Arvieu
Laboratoire de Science du Sol, Institut national de la Recherche Agronomique, 2 place Viala, F-34060 Montpellier Cedex 1, France *

Received 2 November 1995. Accepted in revised form 22 May 1996

Key words: agar gel, color indicator, pH mapping, pH rhizosphere, spectrodensitometry, video camera

Abstract

The colored pH indicator method introduced by Weisenseel et al. (1979) is particularly useful for localizing the zones along roots where acidification/alkalinization occurs. It can also be used to assess the direction and intensity of the proton fluxes. Because the method has not been quantitatively evaluated, however, it is nowadays little used or used in conjunction with other such as potentiometry. In the present study we examine the theoretical basis underlying this method of colorimetric visualization and show its similarity to spectrodensitometry. It thus becomes possible to quantify the luminous information and express it in terms of environmental pH. We describe the method used, emphasizing in particular the conditions required to achieve maximum accuracy of measurement, and an appropriate experimental device. pH distribution around roots can be mapped with a relative error of 0.03 pH units. The experimental device is easy to use and incorporates a computer-controlled video camera, thanks to which all acquisition and calculation procedures can be automated.

Introduction

Exchange activity in plant roots has the effect of altering rhizosphere pH (Haynes, 1990). These pH changes vary considerably, not only according to plant species and environmental conditions, but also according to the physiological state of the plant, the root type and the position along the root (Marschner and Römheld, 1983; Marschner et al., 1986; Pilet et al., 1983). Both the direction and intensity of the pH changes induced may thus vary markedly within the rooting medium. Because of root development, the same elementary volume of rhizosphere may subsequently undergo acidification then alkalinization, or vice versa, with intensity varying according to the type and state of the system examined. It is clear that such root-induced physicochemical dynamics will have a considerable effect on overall rhizosphere behaviour, in particular on the dynamics of highly pH dependent substances such as Al or P compounds. A good understanding of root/soil interactions thus involves not only quantifying but also localizing the fluxes of mineral ions and in particular protons along the roots.

This realization has led several authors to develop various methods for measuring the H^+ fluxes along roots. Most of these methods depend on the use of microelectrodes positioned at the desired measurement sites: this is the case with micropotentiometry, for instance, the usefulness of which has already been more than adequately demonstrated (Gijsman, 1990; Haussling et al., 1985; Schaller, 1987). These microelectrodes are usually very sensitive, being derived most often from well-investigated traditional technologies, but they give information about the system's behaviour only locally in specific points. To overcome this difficulty, Weisenseel et al. (1979) introduced a simple method of visualizing root activity, based on the use of a non-toxic color indicator to show the pH of the growing medium. Easy to use and indicating the behaviour of an entire root system in a single operation, this 'colored pH indicator' method has enjoyed considerable success and enabled major advances to be made in understanding rhizosphere behaviour. However, the method has never been quantitatively evaluated

* FAX No: +33 67632614

and has often been used only to complement point-by-point quantitative methods like micropotentiometry (Gollany and Schumacher 1993; Haussling et al., 1985).

The color indicators most widely used in this field are bromocresol green, bromocresol purple and phenol red (Dinkelaker et al., 1994). Ruiz and Arvieu (1991) have shown that the optical properties of these three indicators are such that there is a precise relationship between optical density and pH when in solution. It is thus possible to accurately calculate the pH of such solutions if the optical density is known. The objective of this paper is an improvement to the 'colored pH indicator' method and an experimental device for measuring pH distribution in translucid films such as agar gels. The device employs a video camera to capture information and can be used to simultaneously localize and quantify with considerable accuracy the pH variations induced by roots.

Materials and methods

pH measurement by spectrodensitometry

Bromocresol green, bromocresol purple and phenol red are three sulphonephthaleins acting as weak acids in water, with pK's of 4.69, 6.40 and 7.79 respectively (Ruiz and Arvieu, 1991). They change color in accordance with H^+ concentration in solution as a result of shifts in the equilibrium between their phenolic and quinonic forms, the effect of protonation/deprotonation, and as a result of the optical properties of the two forms (Cooper, 1977). If x is the molar fraction of the indicator in acidic form and K the indicator's equilibrium constant, proton activity H^+ in dilute solution (where there is little difference between concentration and activity) can be written as:

$$\{H^+\} = x\,[1-x]^{-1}\,K \qquad (1)$$

The optical density, D, of the solution is determined by the proportion of each form present at any given wavelength for a given concentration of indicator, as shown by the relation:

$$D = x\,D_A + [1-x]\,D_B \qquad (2)$$

where D_A and D_B are the optical densities of the acidic and basic forms respectively. By combining Equations (1) and (2) we can write:

$$\begin{aligned} x &= \{H^+\}\,[K + \{H^+\}]^{-1} \\ &= [D - D_B]\,[D_A - D_B]^{-1} \end{aligned} \qquad (3)$$

and then express $\{H^+\}$ in solution and pH versus optical density as:

$$\{H^+\} = K\,[D - D_B]\,[D_A - D]^{-1} \qquad (4)$$

$$pH = -\log(\{H^+\}) \qquad (5)$$

Relative error $\Delta\{H^+\}\,\{H^+\}^{-1}$ and pH error, ΔpH, are respectively:

$$\begin{aligned} &\Delta\{H^+\}\,\{H^+\}^{-1} = [D_A - D]^{-1}\Delta D_A \\ &+[D - D_B]^{-1}\Delta D_B + [[D_A - D]^{-1} \\ &+[D - D_B]^{-1}]\Delta D \end{aligned} \qquad (6)$$

$$\Delta pH = [Ln(10)]^{-1}\,\Delta\{H^+\}\{H^+\}^{-1} \qquad (7)$$

If the experimental error in optical density measurements is constant, i.e. $\Delta D = \Delta D_A = \Delta D_B$, Equation (6) can be written in the form:

$$\begin{aligned} &\Delta\{H^+\}\,\{H^+\}^{-1} \\ &= 2[D_A - D_B][D_A - D]^{-1}[D - D_B]^{-1}\Delta D \end{aligned} \qquad (8)$$

Figure 1 shows pH against optical density, D, (Fig. 1a) and ΔpH against [pH - pK] (Fig. 1b) for any given wavelength. The ΔpH error is symmetrical, and least when [pH - pK] = 0, in other words when $[D - D_B]\,[D_A - D_B]^{-1} = 0.5$, i.e. when $D = 0.5\,[D_A + D_B]$. The equation for ΔpH then becomes:

$$\Delta pH = 8[Ln(10)]^{-1}[D_A - D_B]^{-1}\Delta D \qquad (9)$$

pH measurements should therefore be carried out at the wavelength where the dynamic of optical density $[D_A - D_B]$ for the indicator is greatest, in order to minimize error.

This is the principle on which all spectrodensitometers operate. Optical density is generally measured using a weak beam of light, with the light source and the photomultiplier physically connected. This technique ensures good spatial resolution and accuracy of

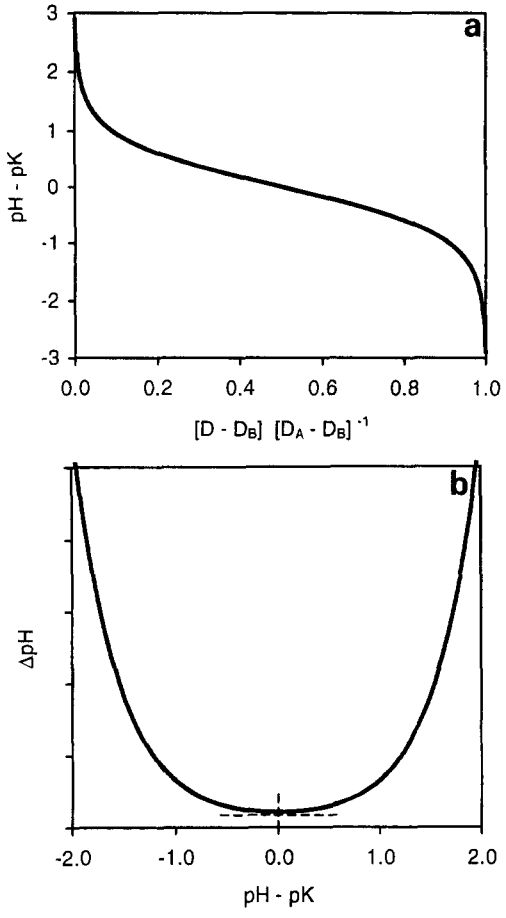

Figure 1. Relationship between pH and optical density D for a solution containing a color indicator. (**a**) Graph of pH as a function of optical densities D, D_A and D_B for the solution analyzed and for acidic and basic solutions containing the same concentration of indicator and measured at the same wavelength. (**b**) Graph of pH error as a function of measured pH. Error is lowest when [pH - pK] = 0.

measurement but limits its use with point-by-point or linear measurement.

pH measurement using a scanning video camera

It is possible to overcome this limitation in 2D image capture by using a scanning video camera. Most commercial cameras these days incorporate a CCD-sensor. The device consists of a dense array of photosites which are individually addressed when the stored charges are read out, thus providing a precise positioning of the photosensor locations (Jarvis, 1988). CCD-sensors are designed for use in imaging and measure light intensity. A computer-controlled video digitizer converts the analog signal into digital data. Most common are 8-bit digitizers, which convert analog signals

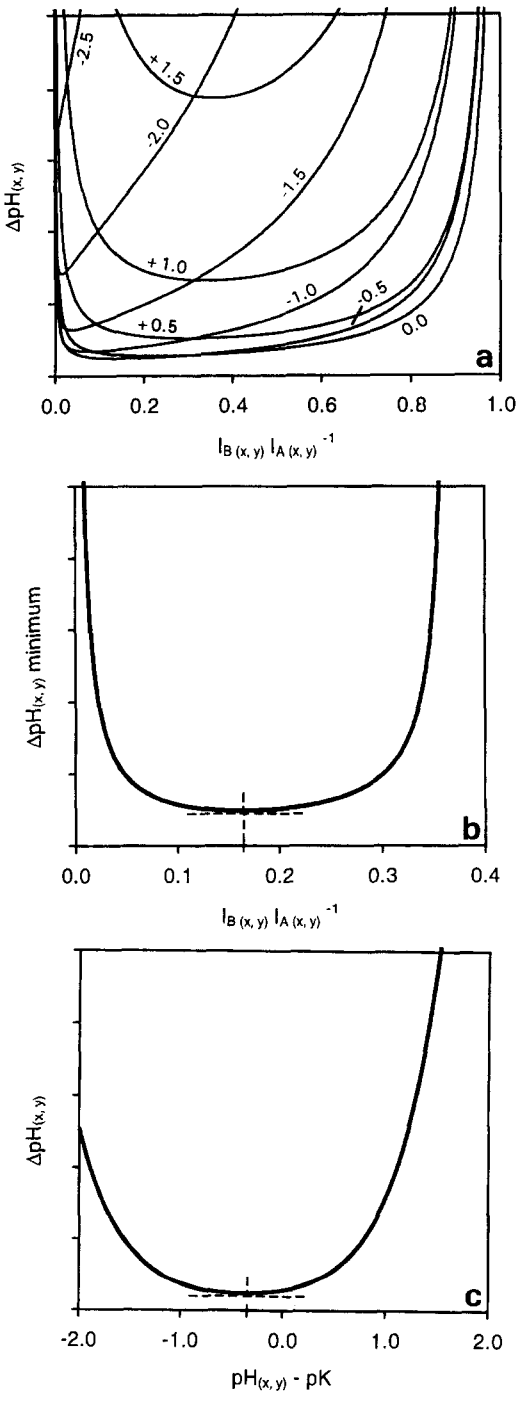

Figure 2. pH error curves as a function of the $I_A\ I_B^{-1}$ ratio for the light intensities of two solutions (acidic and basic) containing the same concentration of color indicator. (**a**) Error curves for different pH values. The values shown on the graph are [pH - pK] values. (**b**) Graph of the minima for the error curves represented in Figure a. (**c**) Graph of pH error as a function of measured pH. When calculated from light intensities, pH error is lowest when [pH - pK] = -0.376.

into 256 (2^8) grey levels, i.e. in the integer values included in the interval 0 to 255. The raw data are therefore a 2D matrix (or images) of integer values $I_{(x,y)}$ for light intensities.

The use of a video camera as captor for optical measurement supposes first that the response curve of the CCD-sensor is linear in the useful range of light intensity. The video camera must be accordingly adjusted and carefully calibrated. Optical density $D_{(x,y)}$ must then be computed from the light intensity $I_{(x,y)}$ measured at any image point $P_{(x,y)}$ (or pixel, for picture element), in accordance with the equation:

$$D_{(x,y)} = -\log(I_{(x,y)}\ I_{O(x,y)}{}^{-1}) \qquad (10)$$

where $I_{O(x,y)}$ is the light intensity of the light source. Equation (10) can be substituted into Equation (4) to give:

$$\{H^+\}_{(x,y)} = K \log(I_{(x,y)}\ I_{B(x,y)}{}^{-1})\ [\log(I_{A(x,y)}\ I_{(x,y)}{}^{-1})]^{-1} \qquad (11)$$

Equation (11) shows that it is not necessary to know the light source intensity I to be able to calculate the pH at any pixel $P_{(x,y)}$, provided that $I_{A(x,y)}$, and $I_{B(x,y)}$ are measured with the same light source intensity $I_{O(x,y)}$. In practice, this means that the relative positions of the light source and the CCD-sensor of the video camera do not vary during experimentation so that each pixel $P_{(x,y)}$ in the images is associated with a given position (x,y) relative to the light source.

Minimization of error in the video camera input signal

The relative error in H^+ concentration is:

$$\Delta\{H^+\}_{(x,y)}\ \{H^+\}_{(x,y)}{}^{-1} = [\mathrm{Ln}(10)]^{-1} [[\log(I_{A(x,y)}\ I_{(x,y)}{}^{-1})]^{-1}\ \Delta I_{A(x,y)}\ I_{A(x,y)}{}^{-1} + [\log(I_{(x,y)}\ I_{B(x,y)}{}^{-1})]^{-1}\ \Delta I_{B(x,y)}\ I_{B(x,y)}{}^{-1} + [[\log(I_{A(x,y)}\ I_{(x,y)}{}^{-1})]^{-1} + [\log(I_{(x,y)}\ I_{B(x,y)}{}^{-1})]^{-1}]\ \Delta I_{(x,y)}\ I_{(x,y)}{}^{-1}] \qquad (12)$$

Equation (12) shows that pH error is proportional to relative errors $\Delta I_{A(x,y)}\ I_{A(x,y)}{}^{-1}$, $\Delta I_{B(x,y)}\ I_{B(x,y)}{}^{-1}$ and $\Delta I_{(x,y)}\ I_{(x,y)}{}^{-1}$. First of all, therefore, it is necessary to minimize the relative error in the video camera input signal. As the light intensities of the images are encoded as integer values included in the interval 0 to 255, the method most commonly used in image analysis is to capture N images of the same object and integrate them immediately when they are captured, so as to widen the acquisition dynamic and therefore the values for $I_{A(x,y)}$, $I_{B(x,y)}$ and $I_{(x,y)}$. With this approach it is not possible, however, to estimate input error and consequently pH error. It is therefore best to consider each image i (where i = 1, 2, ..., N) of optical intensity $I_{i(x,y)}$ as the sum of an image of useful signal $S_{i(x,y)}$ and an image of noise $B_{i(x,y)}$ such that:

$$I_{i(x,y)} = S_{i(x,y)} + B_{i(x,y)} \quad \text{where } i = 1, 2, ..., N \qquad (13)$$

If noise $B_{i(x,y)}$ is assumed to be a random effect, stable over time and with a null average, the signal $I_{(x,y)}$ and the standard deviation $\sigma_{(x,y)}$ of signal calculated for N images will be such that (Marion, 1987):

$$I_{(x,y)} = N^{-1}\Sigma_{i=1}^{n}\ I_{i(x,y)} = N^{-1}\ \Sigma_{i=1}^{n}\ S_{i(x,y)} \qquad (14)$$

$$\sigma_{I(x,y)}{}^2 = N^{-1}\ \Sigma_{i=1}^{n}\ [I_{i(x,y)} - S_{i(x,y)}]^2 = N^{-1}\ \sigma_{B(x,y)}{}^2 \qquad (15)$$

In other words, if N images are captured, it is possible to reduce the associated input noise by a factor of $\sqrt{N}$. The first thing to do in minimising pH error is therefore to capture several images in succession, these being considered as occurrences in the random effect, then calculate the resulting signal image for intensity $I_{(x,y)}$ and the associated error image $\sigma_{I(x,y)}$ for $I_{A(x,y)}$, $I_{B(x,y)}$ and $I_{(x,y)}$ using Equations (14) and (15).

Minimization of error for pH measurements

Secondly, analysis of Equation (12) shows that pH error depends on absolute values of $I_{A(x,y)}$ and $I_{B(x,y)}$. ΔpH tends towards infinity when $I_{B(x,y)}$ tends towards 0 or $I_{A(x,y)}$. ΔpH thus has a minimum value in relation to the $I_{B(x,y)}\ I_{A(x,y)}{}^{-1}$ ratio. Figure 2a shows curves for ΔpH against the $I_{B(x,y)}\ I_{A(x,y)}\ B_{y-1}$ ratio where $I_{(x,y)}$ is such that $[pH_{(x,y)} - pK)]$ is constant. The shape of the curve, and therefore the position of the minimum error, varies greatly according to the $[pH_{(x,y)} - pK]$ value. Figure 2b is a graph of the minima for the ΔpH curves against the $I_{B(x,y)}\ A(x,y)^{-1}$ ratio: ΔpH minima are lowest when $[pH_{(x,y)} - pK] = -0.376$ and $I_{B(x,y)}\ I_{A(x,y)}{}^{-1} = 0.163$. Calculation shows that the curve for ΔpH minimum against $[pH_{(x,y)} - pK]$ is moreover

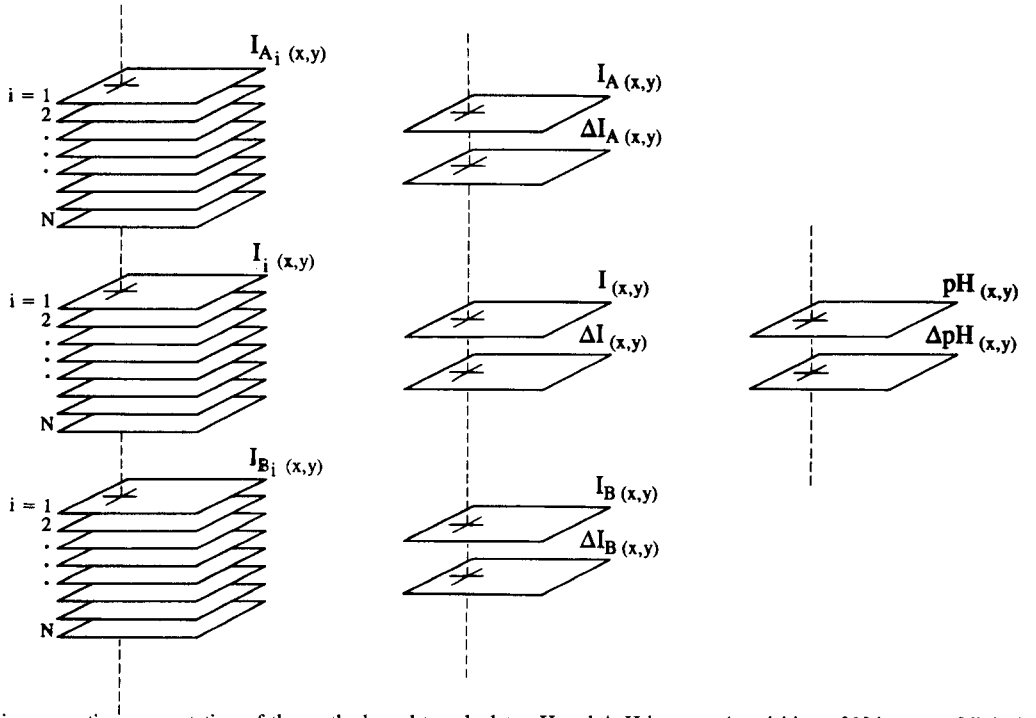

Figure 3. Diagrammatic representation of the method used to calculate pH and ΔpH images. Acquisition of N images of light intensity I_i, calculation of images for mean (signal) I and variance (noise) ΔI, calculation of pH and ΔpH images. All calculations are carried out pixel by pixel $P_{(x,y)}$.

quite symmetrical about this value, making it possible to minimize pH error over a wide pH range. The resulting curves for $\Delta pH_{(x,y)}$ against $[pH_{(x,y)} - pK]$ when $I_{B(x,y)}\ I_{A(x,y)}^{-1} = 0.163$ are presented in Figure 2c. The range of optimum pH measurement is 0.376 pH units lower than the optimum range determined by measuring optical density (see Fig. 1b). If the $I_{B(x,y)}\ I_{A(x,y)}^{-1}$ ratio is optimized, however, a good level of accuracy can be achieved for pH measurements over about 3 pH units, i.e. more or less the same range as when optical density is measured directly.

In order to minimize pH error, it is consequently necessary in practice to adjust the offset and gain of the video camera, before experimentation begins, so that the optimum light intensity ratio $I_{B(x,y)}\ I_{A(x,y)}^{-1}$ is obtained for saturated acidic and basic images for the range of pH values expected in the experiment.

Optical device, hardware and software

Images were obtained using a CCD video camera (Sony XC77CE) connected to an 8-bit video digitizer board (Matrox PIZ 1024) installed in a microcomputer. The video digitizer board enabled 256×256 or 512×512 digital images to be captured. Monitoring devices included two control screens, one of which was connected directly to the digitizer board and used to display either the images conveyed by the camera or those stored in the digitizer board memory, while the other was connected to the computer and used as a standard control screen. The optical device consisted of a zoom lens (Canon V6×16 -1:9 macro) fitted with a narrow bandwidth interference filter (Optometrics Corporation Inc.) The light source was a PTB-500 pattern box (Kyoritsu Electric Company Ltd) adjusted to a color-temperature of 3200 K and a luminance of 706 candela m^{-2}. The pattern box and video camera were aligned and secured. Camera control, image managenent and computations based on the captured images were handled by programs specially written in C language and included in the image analysis software Visilog v.3.61 (Noesis).

Calibration of video camera

The video camera was calibrated using sheets of tracing paper. Its transfer function was determined by using the SAS v.4 software's NLIN procedure to fit the curve for real light intensities I versus measured values J to the model:

$$I = J\,[1 + a[Ln(J) - b]\,[Ln(J) - Ln(J_A)]\,[Ln(J) - Ln(J_B)]] \qquad (16)$$

where J_A and J_B are the highest and lowest light intensity readings and a and b the adjustment constants. This empirical model was chosen simply because it gives good adjustment of the transfer function while of necessity satisfying the conditions $I(J_A) = J_A$ and $I(J_B) = J_B$.

The calibration of video camera must be done once and for all: it must be done very carefully because the transfer function of most cameras are not perfectly linear and the absolute accuracy of the method depends on it.

Preparation of calibration, standards and samples for pH mapping

The basic device consists of a trough made of two rectangular sheets of glass separated and kept parallel to one another by strips of PVC. Sheet size depends on the experimental area required. 100x200 mm sheets were used in these experiments. Thickness of strip is likewise chosen to suit requirements: in these two experiments it was 3 mm, but it can be different.

pH distribution was measured on thin films of agar or agarose gel. The films were prepared by adding 10 g of agar powder (Prolabo) or agarose powder (Fluka Ref 05068) (Calba et al., 1995) and 30 mg of bromocresol purple or bromocresol green per litre of solution. The mixture was boiled for several minutes, then cooled to 37 °C in a water bath. The solution was then poured into the trough. To study root behaviour, the seedling's root system was first positioned between the two glass sheets, then the gel was poured over it. One of the glass sheets was then removed so as not to confine the root environment. Two saturated calibration standards (basic and acidic respectively) also had to be produced for each series of measurements.

It should be noted that the method is based on measurements of optical density. The optical density of the gel film for a given pH is determined both by its concentration of color indicator and by its thickness (in fact, by the product of its concentration and the optical way through the medium in accordance with Beer-Lambert's law). It follows that it is preferable to produce all the films, both samples and calibration standards, using the same original solution. The troughs should likewise be constructed with considerable care to ensure that thickness is as near the same as possible from one film to the next and that the entire surface of each film has a constant thickness.

Optical device and video camera adjustment

Readings are taken in a darkroom to avoid stray light. The optical device and the video camera have to be adjusted before the start of any experiment. The two saturated calibration standards (acidic and basic) are placed side by side in the camera field against the pattern box. The zoom aperture is then adjusted to avoid both low and high saturation of the CCD-sensor. Focusing of image is adjusted using a target drawn on a transparent sheet.

The video camera's offset and gain are then adjusted to give the optimum measured light intensity ratio for the saturated acidic and basic images $\alpha = I_B\ I_A^{-1}$ for the anticipated range of pH values. This step has been automated, as accurate manual adjustment is difficult. Two masks, A and B, are defined, corresponding to the acidic and basic zones of the image containing the two calibration standards. The standards are placed so that each occupied an equivalent area of the camera field, i.e. so that the numbers of pixels for the two masks, N_A and N_B, are much the same, and the value required for I_A and I_B are entered. An I_A value of 235 is chosen to avoid saturation above grey level 255. The I_B value was then computed as $I_B = \alpha\ I_A$. The algorithm used is an iterative adjustment by dichotomy of two camera values, gain and offset, simultaneously. At each step, the number of images captured is the same as the number of new gain and offset pairs tested. The corresponding pairs of mean measured intensities J_A and J_B are calculated as:

$$J_A = N_A{}^{-1}\ \Sigma_{NA}\ J_{A(x,y)} \quad \text{if } P_{(x,y)} \text{ included in mask A,} \qquad (17)$$

$$J_B = N_B{}^{-1}\ \Sigma_{NB}\ J_{B(x,y)} \quad \text{if } P_{(x,y)} \text{ included in mask B,} \qquad (18)$$

where N_A and N_B are the numbers of pixels in masks A and B. The measured intensities J_A and J_B are then compared to the given intensities I_A and I_B. The stop condition is: no change in $|J_A - I_A|$ and $|J_B - I_B|$ values between two steps. Convergence is reached when $J_A = I_A$ and $J_B = I_B$.

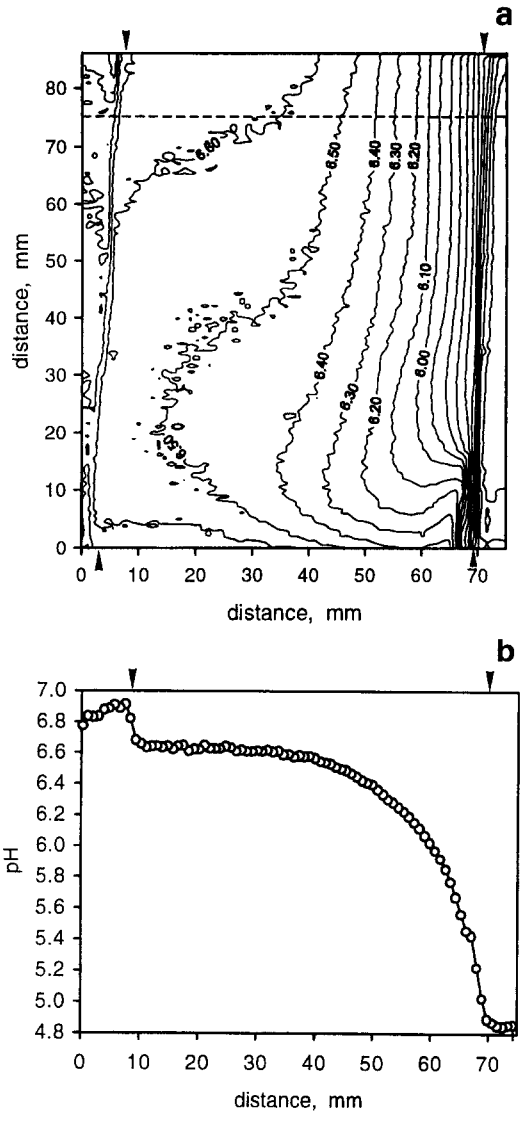

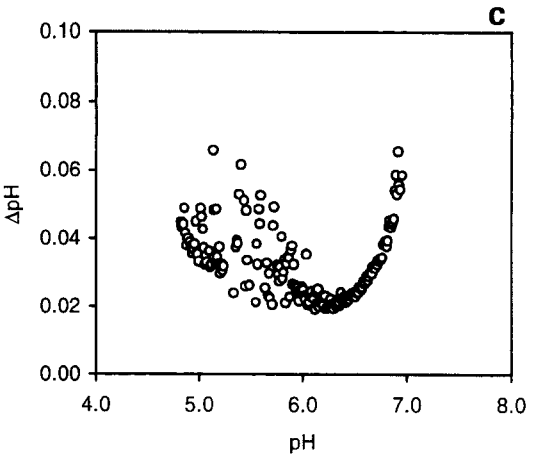

Figure 4. Experiment to examine H^+ diffusion in agar film between two dialysis tubes with a constant pH of 4.8 and 6.8 respectively (1 m*M* KCl medium). (**a**) pH image after 48 h of operation of the device. Contact lines between the dialysis tubes and the agar film are reported by arrows. (**b**) pH profile produced via the pH image (dotted line on Fig. a). (**c**) Graph of mean measurement error as a function of measured pH.

Image capture and pH mapping

The optical device and video camera were first adjusted as previously described. The pH mapping was then conducted on the gel layers using an automated acquisition process for greater convenience. Standard and sample agar layers were placed one after the other directly in the camera field. Once a sample had been correctly positioned, the required sequence of N integer images was captured and stored in computer memory. The resulting real images for signal and noise were then calculated using Equations (14) and (15) and stored in permanent form. All data presented here were obtained from N = 25 images.

At the end of the capture session, signal images were corrected using the transfer function (16). The corresponding pair of pH and ΔpH images was then computed using Equations (11) and (5) or (12) and (7), respectively. The same standard images were used for all sample images in the experiment. Figure 3 shows the acquisition process in summary form.

Results and discussion

Figures 4 and 5 present two experiments clearly illustrating the advantages and limitations of the method of pH measurement described here. The first experiment studies the diffusion of a KCl solution in agar film to evaluate the buffer capacity of the substrate and its effect on the H^+ diffusion. Its interest is to illustrate a physical application of the method which required pH measurement on a wide range of pH (about 2 pH units). The second experiment illustrates the main use envisaged, i.e. quantification and localization of the H^+ fluxes along roots. In this application, the pH variations are less than 0.5 pH units and the relative accuracy on measurement becomes essential.

Study of H^+ diffusion in agar gel

The experimental device consisted of an agar film located between two parallel dialysis tubes 70 mm

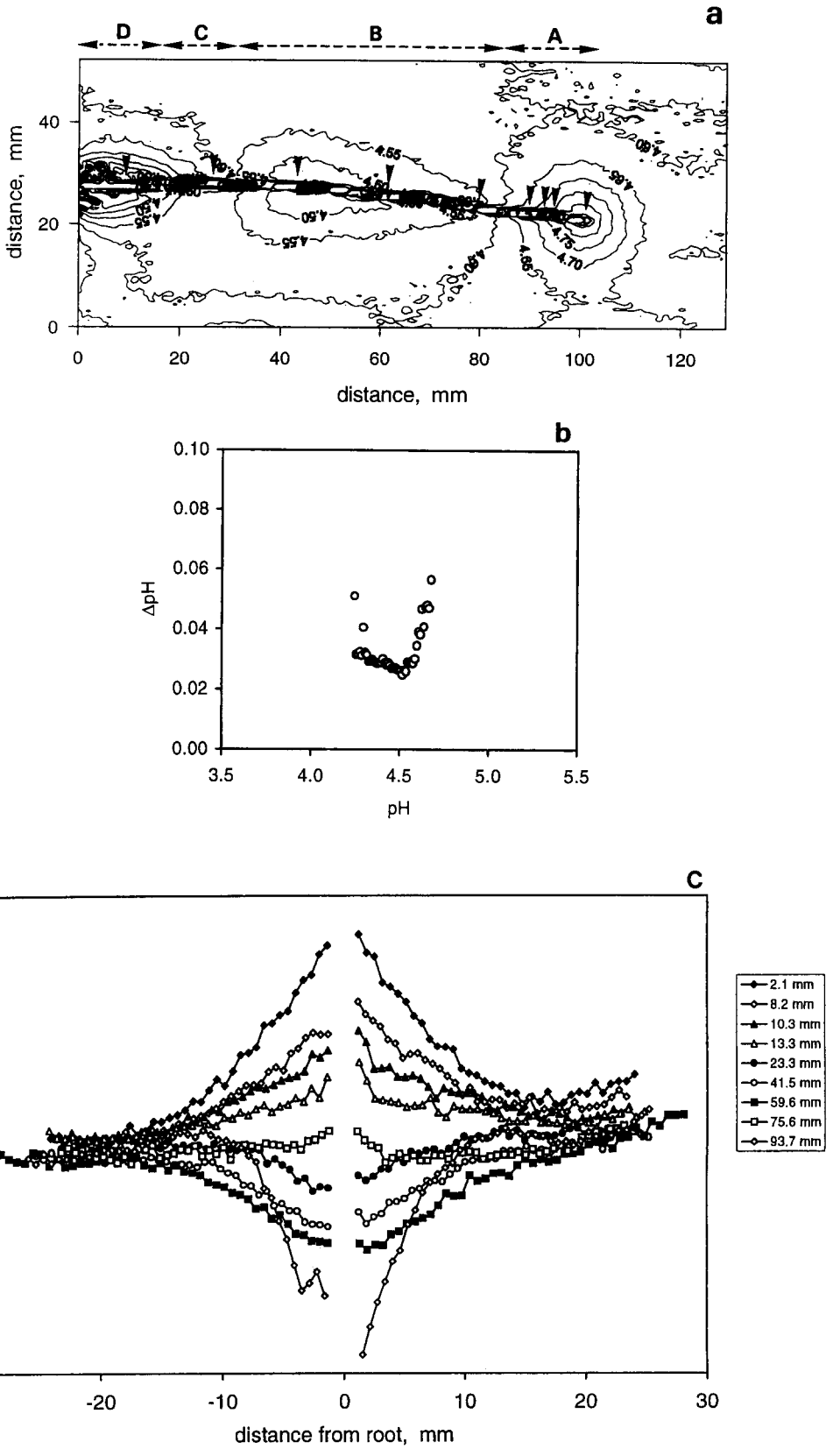
a
D
C
B
A
distance, mm
0
20
40
distance, mm
0
20
40
60
80
100
120
4.55
4.50
4.55
4.60
4.65
4.70
4.75
b
ΔpH
0.10
0.08
0.06
0.04
0.02
0.00
3.5
4.0
4.5
5.0
5.5
pH
c
pH
4.9
4.8
4.7
4.6
4.5
4.4
4.3
-30
-20
-10
0
10
20
30
distance from root, mm
2.1 mm
8.2 mm
10.3 mm
13.3 mm
23.3 mm
41.5 mm
59.6 mm
75.6 mm
93.7 mm

apart. 1 m*M* KCl solutions, the pH of which had been adjusted to 4.8 and 6.8 by the addition of HCl or KOH, circulated continuously through each of these tubes. The agar film itself was initially produced using a 1 m*M* KCl solution with a pH of 6.8. The color indicator used was bromocresol purple, which has a pK of 6.40. The measurements were then carried out at a wavelength of 589 nm. The gel and percolating solutions were given the same concentration of color indicator in order to keep its concentration in the agar film at a constant level. The whole device was located between two parallel strips of glass 3 mm apart. The calibration standards were 100×150×3 mm saturated acidic and basic films of agar.

Figure 4a shows the image of the pH values calculated for the whole device after 48 h of operation, while Figure 4b shows a profile produced via this image. Automation of the acquisition and calculation procedures make it possible to calculate a value for each pixel contained in the images. As far as pH is concerned, only the values of the agar film between the dialysis tubes are meaningful, however only this area of the image meets the methodological requirement that sample and calibration standards should have the same basic optical characteristics. This is not so for the areas representing the dialysis tubes containing the percolating solutions, as the equivalent of these areas on the calibration standards is in fact agar film. Although the pixel values for the dialysis tubes are quite close to the pH values expected, optical density being very low for both the tubes and the agar, they are nevertheless distorted and should not, in fact, be taken into consideration when results are interpreted. This method, perhaps more than others, clearly requires a full awareness of the experimental conditions because it is image-based, and this gives it a particularly strong visual aspect.

Figures 4a and b show that a pH gradient of between 5.4 and 6.6 was established in the agar film after 48 h of operation. The phenomenon can be analyzed in conventional fashion using the profile (Fig. 4b); but the pH map (Fig. 4a) also shows a spatial heterogeneity in the device's operation. Observation suggests that this is caused by variations in the degree of contact between the dialysis tubes and the gel. Figure 4c shows the mean pH error relative to measured pH: this curve is obtained by calculating the mean ΔpH for all pixels in the pH map. Under these experimental conditions and for the measurement range ($5.4 < pH < 6.6$), the mean error is of the order of 0.03 pH units. As previously indicated, this measurement error depends in part on the quality of the camera's gain and offset adjustment, which enables the $I_B\ I_A^{-1}$ ratio to be optimized, and in part on the sensitivity of the signal acquisition system, i.e. of the CCD video sensor - digitizer board unit. The experiment shows that, with the equipment used, the acquisition of 25 successive images coded over 256 grey levels enables input noise to be reduced to 0.25 of a grey level, i.e. to a relative input error of the order of 10^{-3} (signal/noise ratio =1000). A good standard of measurement, more than adequate for most applications, is thus achieved.

Localization of H^+ effluxes along roots

The equipment for quantifying and localizing the H^+ fluxes along roots consisted of a 7 d-old maize seedling cultivated in a 1 m*M* KNO_3 solution with a pH of 4.6 (Fig. 5). The color indicator used was bromocresol green, which has a pK of 4.69. The measurements were then carried out at a wavelength of 612 nm. The diffusion medium was a 1 m*M* KNO_3 agarose gel with a pH adjusted to 4.6 by the addition of 0.1 m*M* HCl. Moreover, the upper glass sheet used for pouring the film was removed so as not to confine the root environment. Figure 5a represents the pH map obtained after 2 h of contact between the root and the agarose gel: it shows where acidification/alkalinization occurs along the root relative to its age. Four different areas of activity can be distinguished between the tip of the main root and the base of the plant stem: (i) the tip, which alkalinizes the environment, (ii) the mature zone, which acidifies the environment, (iii) an intermediate zone located 20–30 mm from the base of stem, where the pH of the environment is unchanged or only slightly changed, (iv) the area next to the base of stem, which strongly acidifies the environment. Morphological observation of the root shows that areas (iii) and (iv) correspond to

Figure 5. Experiment to localize H^+ fluxes along a maize root grown in 1m*M* KNO_3 medium with a pH of 4.6. (**a**) pH image after 2h of contact between root and agarose gel (A: tip and elongation zone of main root; B: mature zone of main root; C: emergence zone of 2nd order roots; D: elongation zone of 2nd order roots). (**b**) Graph of mean measurement error as a function of measured pH. (**c**) pH profiles produced at right angles to the axis of the main root 2.1, 8.2, 10.3, 13.3, 23.3, 41.5, 59.6, 75.6 and 93.7 mm respectively behind the main root tip. The profile positions are reported by arrows on Figure 5a.

the emergence and elongation zones for second order roots.

Figure 5b shows the pH error relative to measured pH: it is comprized between 0.025 and 0.050 pH units on the whole rooting medium. Figure 5c presents pH profiles obtained at different places along the root. All were obtained at right angles to the axis of the main root. The pH readings varied by no more than 0.25 pH units above or below the medium's initial pH which was in the vicinity of 4.6. The method is sufficiently sensitive to evaluate these pH variations accurately along the full length of the main root: alkalinization at the tip (Fig. 5c: 2.1, 8.2, 10.3 and 13.3 mm profiles) and acidification in the mature zone (23.3, 41.5 and 59.6 mm profiles), slight alkalinization in the emergence zone for second order roots (75.6 mm profile) and strong acidification in the elongation zone for second order roots (profile 93.7 mm from the tip). It should be noted that the shape of this last profile confirms the alkalinization of the medium by the tips of second order roots. The profile is characterized by a steep pH gradient which can only be produced by two contradictory sources in close proximity: these will be the elongation zones for second order roots (between 0 and 10 mm from the main root), which tend to acidify the medium, and the tips of these same second order roots (10–15 mm from the main root), which have an alkalinizing effect. These results are in agreement with the results obtained by Weisenseel et al. (1979) and O'Neill and Scott (1983).

Figure 5c also shows an experimental bias that is difficult to avoid and hence frequently observed. The background pH value measured to the left of the root is on average 4.60, precisely the same as that of the initial solution, while the value measured to the right of the root is systematically about 0.03 pH units higher. The discrepancy is the result of a slight difference in the thickness of the agarose film on either side of the root., which is due to a fault in the arrangement for keeping the glass sheets apart at the time the film was produced. In general terms, the thinner the film being analyzed, the greater the relative importance of this experimental bias.

Conclusion

The 'colored pH indicator method' introduced by Weisenseel et al. (1979) is similar to conventional colorimetric methods. The luminous information can thus be quantified and expressed in terms of pH if the colored film is analyzed using spectrodensitometry methods. The experimental device described uses a video camera to capture information, and this has several advantages. The equipment is relatively inexpensive and simple to use. In addition, if connected to a computer, a video camera can be controlled via software and the images digitized immediately when they are acquired. These features make it possible to automate all acquisition and calculation procedures, thus considerably lightening the researcher's workload. In particular, they enabled us to optimize the conditions of acquisition and so reduce considerably instrumental relative error on pH measurement: about 0.03 units over a wide range of pH, which is certainly less than the whole experimental error in most applications. The method of pH measurement by videodensitometry presented here provides a high standard of performance and is well suited to the study of root-induced pH variation. This method can be used not only to localize but also to quantify directly the H^+ fluxes along roots.

Acknowledgements

We thank Gérard Souche and Simone Combettes for their technical support, Olivier Douarche and Nathalie Paget for their helpful assistance in computer work.

References

Calba H, Jaillard B, Fallavier P and Arvieu J C 1995 Agarose as a suitable substrate for use in the study of Al dynamics in the rhizosphere. Plant and Soil 178, 67–74.

Cooper T G 1977 The tools of biochemistry. John Wiley, New York, USA. 423 p.

Dinkelaker B, Hahn G, Römheld V, Wolf G A and Marschner H 1994 Non-destructive methods for demonstrating chemical changes in the rhizosphere I. Description of methods. Plant and Soil 155/156, 71–74.

Gijsman A J 1990 Rhizosphere pH along different root zones of Douglas-fir (*Pseudotsuga menziesii*), as affected by source of nitrogen. Plant and Soil 124, 161–167.

Gollany H T and Schumacher T E 1993 Combined use of colorimetric and microelectrode methods for evaluating rhizosphere pH. Plant and Soil 154, 151–159.

Haussling M, Leisen E, Marschner H and Römheld V 1985 An improved method for non-destructive measurements of the pH at the root-soil interface (rhizosphere). J. Plant Physiol. 117, 371–375.

Haynes R J 1990 Active ion uptake and maintenance of cation-anion balance: a critical examination of their role in regulating rhizosphere pH. Plant and Soil 126. 247–264.

Jarvis L 1988 Microcomputer video image analysis. J. Microsc. 15, 83–97.

Kochian L V, Shaff J E, Kühtreiber W M, Jaffe L F and Lucas W J 1992 Use of an extracellular, ion-selective, vibrating microelectrode system for the quantification of K^+, H^+, and Ca^{2+} fluxes in maize roots and maize suspension cells. Planta 188, 601–610.

Marion A 1987 Introduction aux techniques de traitement d'images. Eyrolles, Paris, France. 267 p.

Marschner H and Römheld V 1983 In vivo measurement of root-induced pH changes at the soil-root interface: effect of plant species and nitrogen source. Z. Pflanzenernaehr. Bodenkd. 111, 241–251.

Marschner H, Römheld V, Horst W J and Martin P 1986 Root-induced changes in the rhizosphere: importance for the mineral nutrition of plants. Z. Pflanzenernaehr. Bodenkd. 149, 441–456.

O'Neill R A and Scott T K 1983 Proton flux and elongation in primary roots of barley (*Hordeum vulgare* L.) Plant Plysiol. 73, 199–201.

Pilet P E, Versel J M and Mayor G 1983 Growth distribution and surface pH patterns along maize roots. Planta 164, 96–100.

Ruiz L and Arvieu J C 1990 Measurement of pH gradients in the rhizosphere. Symbiosis 9, 71–75.

Schaller G 1987 pH changes in the rhizosphere in relation to the pH-buffering of soils. Plant and Soil 97, 444–449.

Weisenseel M H, Dorn A and Jaffe F J 1979 Natural H^+ currents traverse growing roots and root hairs of barley (*Hordeum vulgare* L.). Plant Physiol. 64, 512–518.

Section editor: A C Borstlap